Proceedings of the 17th
IEEE International Conference on Nanotechnology
Pittsburgh, USA, July 25-28, 2017

Nanostructured Miniaturized Artificial Magnetic Conductors (AMC) for High-Performance Antennas in 5G, IoT, and Smart Skin Applications

Tong-Hong Lin, P. Markondeya Raj, Atom Watanabe, Venky Sundaram, Rao Tummala, and Manos M. Tentzeris

***Abstract*—The emergence of fan-out packaging for 5G and IoT applications has brought escalating performance concerns that arise from the proximity of radiating components such as antennas to lossy materials such as metals and silicon. These concerns also arise in wearable ("smart skin") electronics where the human tissues act as the lossy substrate. Artificial magnetic conductors (AMC) are widely explored for enhancing the performance of antennas that are in close proximity to metallic surfaces and other lossy substrates such as silicon and human tissue. High-permittivity or high-permeability materials can be used to significantly reduce the sizes of AMCs. Nanostructured materials provide unique opportunities to provide stable properties up to the GHz and mm-Wave frequency ranges. In this paper, novel miniaturized nanostructured AMCs utilizing Barium Strontium Titanate (BST) thinfilms and ceramic-polymer composites are demonstrated through full-wave modeling analysis. The size reduction rates are 50.6 % when using 3 µm of BST thinfilm and 77 % when using 400 µm of ceramic-polymer composites. This concept can be further extended with high-permeability magnetic films, and thicker nanocomposite films to achieve further size and performance improvement for a variety of frequency bands and applications.**

***Index Terms*—Nanostructured, artificial magnetic conductors (AMC), Frequency-selective surfaces (FSS), BST, high permittivity, thin film, miniaturization, millimeter-wave, GHz;**

I. Introduction

There has been a growing demand for miniaturized Radio Frequency (RF) systems in sensing, detection, identification and communication applications in the last few decades. Examples of these applications include Gb/s local-area and wide area-networks, mm-wave automotive radar, imaging in the mm-wave and THz frequencies, wireless sensor networks, Radio Frequency Identification (RFID) and other multiple access communication systems [1]. It is estimated that over 50 billion devices will be connected to the internet by 2020, in contrast to the current number (2017) of 28.4 billion devices. Moving towards 5G is a natural course, as higher data rates and higher densities of connected devices per unit area are increasingly desired. The key system technologies enabled by 5G technology are classified as: (a) Wi-Fi Cellular and Backhaul Communications, (b) V2X communications for ADAS, (c) Internet of Things (IoT), (d) Massive MIMO, (e) Cognitive Radio.

T.-H. Lin, and M. M. Tentzeris are with the School of Electrical and Computer Engineering, Georgia Institute of Technology, Atlanta, GA, 30332-250 USA (e-mail: tlin97@ gatech.edu).

P. M. Raj, A. Watnabe, V. Sundaram, and R. Tummala are with the Packaging Research Center, Georgia Institute of Technology, Atlanta, GA 30332-0560 USA (e-mail: raj@ ece.gatech.edu).

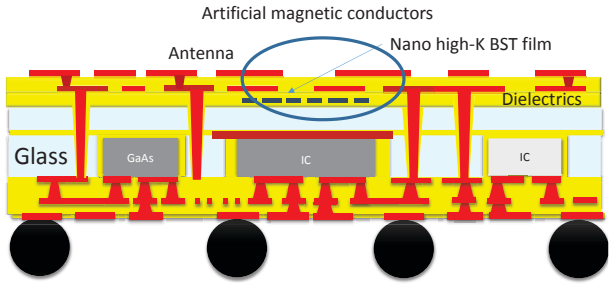

Figure 1. Conceptual cross-section of glass fan-out package with nanostructured AMCs to suppress proximity effects between antenna and metal or lossy semiconductor elements.

For optimal performance, the commonly-used patch antennas typically need to be integrated into the substrate with active circuits using low-loss interconnects and feedlines. The evolution of embedded wafer fan-out packaging (eWFO), also referred to as embedded wafer-level ball grid array (eWLB) or fan-out wafer-level packaging (FO-WLP), has further enhanced the performance of organic mm-wave packages [2]. eWFO eliminates the use of wire bonding parasitic, which brings in two benefits: 1) significantly reduced parasitic compared to the standard BGA-wirebond and BGA flip-chip packages, and 2) reduced foot-print and thickness for high pin-count dies. Glass-based fan-out packages are emerging as an alternative to eWFO in order to realize mm-wave technologies because of their superior dimensional stability, availability in large-area low-cost panels, ability to form fine-pitch through-vias, stability to temperature and humidity, and matched coefficient of thermal expansion (CTE) with devices, along with low dielectric loss compared to silicon and mold compounds commonly used in fan-out packages [3]. A fan-out package with an antenna placed on top of embedded ICs is shown in Figure 1.

Integrating antennas with packages has been recently becoming increasingly popular. However, direct integration of antennas on silicon or metallic surfaces typically leads to a decrease in the radiation efficiency and performance of the antennas. Hence, additional modifications are required. High-impedance surfaces (HIS) provide a favorable radiation environment alleviating these issues. Frequency-selective surfaces (FSS) are also utilized to selective transmit or reflect certain frequencies [4]. These are typically two-layer structures of metals and dielectrics that create impedance

matching or resonance conditions at certain frequencies. FSS effectively comprise of a distributed network of embedded capacitors and inductors that are formed over the redistribution layers of the fan-out embedded active devices. Such structures can be used to form artificial magnetic conductors (AMC), while being also used as antenna grounds in RFID tags [5].

AMC structures using traditional dielectrics do not feature adequate high permittivity or permeability, usually resulting in physically large component designs. This makes them incompatible with the antenna and chip dimensions. On the other hand, traditional high-permittivity and high-permeability films do not have stable properties in GHz frequencies.

In this paper, a novel AMC structure for 5G and IoT applications is designed and simulated. Ceramic-polymer composite or a thin film of BST is inserted into the substrate to reduce the size of the AMC structure. By utilizing nanoscale superparaelectric films, the frequency stability can be significantly enhanced to make them operate at bands up to above 30 GHz. Moreover, with such films, the unit-cell size of the AMC structure can be reduced significantly so that the size is small enough to be integrated with chips and packages.

II. Nanostructured Material Candidates for AMCs

Nanomaterials feature superior electrical properties for capacitors and thus lead to miniaturized high-Q multilayer passives with higher dielectric constant and low TCC, wideband and low-loss interconnects. They also show superior magnetic properties from improved exchange coupling between the magnetic domains, absence of leakage, absence of domain wall assisted relaxation etc. These nanostructures are expected to result in higher permittivity and permeability at much higher frequencies.

High-permittivity films are processed either as ceramic thinfilms or as ceramic-polymer composite films. For ceramic films, the permittivity can vary from 300-1000 but integrating them generates manufacturing challenges. On the other hand, ceramic-polymer composites have only a permittivity of 15-20 but are easy to integrate as thick films. The low permittivity is because of the inherent depolarization of the particles and the presence of a polymer dielectric medium that further lowers the permittivity. Both ceramic-polymer composite films and ceramic films are considered in this paper. Integrating such films on glass substrates has been demonstrated by the authors in an earlier work [6].

The superior dielectric characteristics of nanoscale ferroelectric films are believed to originate from the existence of PNR (polar nanoregions). The existence of PNR has been clearly illustrated through Raman spectroscopy [7]. The microwave characteristics in this case are attributed to the inhomogeneous distribution of oxygen vacancies in PNR. The wide distribution of hopping distances or hopping energies result in broad relaxation bands. The dielectric behavior in this frequency range has been attributed to the Curie–von Schweidler relaxation [7], which is written empirically as:

$$\varepsilon' \propto \frac{1}{f^{1-n}} \quad (1)$$

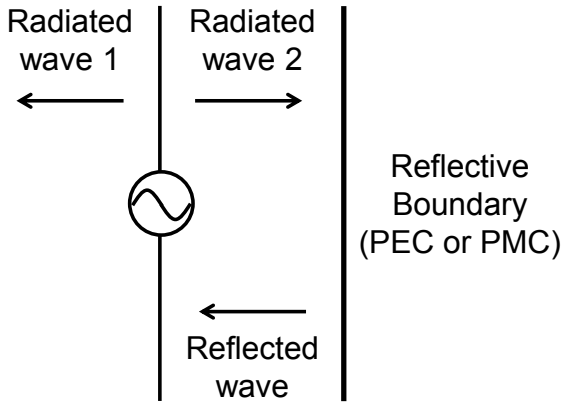

Figure 2. An antenna located close to a reflective boundary

$$\varepsilon'' \sim \cot(\frac{n\pi}{2}) \quad (2)$$

Such nanostructured ferroelectrics have been shown to exhibit frequency stability beyond 20 GHz [8].

Nanostructured magnetic films have been also shown to be effective in GHz frequencies unlike traditional magnetic films, while also retaining permeability of above 1. The FMR frequency for an anisotropic magnetic thin-film is:

$$F_{fmr} = \frac{\gamma}{2\pi}\sqrt{(M_s + H_k)H_k} \quad (3)$$

where H_k is the anisotropy field (a combination of magnetocrystalline anisotropy, shape anisotropy and external field anisotropy), Ms is the saturation magnetization, and γ is the gyromagnetic ratio. Therefore the FMR is improved by a factor of at least $\sqrt{\mu}$ for films with strong magnetic field anisotropy. By introducing shape anisotropy with rectangular nanoarrays or an external field bias, the FMR can be further enhanced to GHz frequencies [9].

III. Nanostructured AMCs

A. Theories and Applications of AMCs

The AMC structures can be used in a lot of applications such as high performance antenna, IoT, and smart skin. The basic principles are briefly introduced first. The radiated and reflected waves of an antenna that is located close to a reflective boundary are shown in Figure 2. The ratio of E-field of the reflected wave and the radiated wave 2 can be calculated as:

$$\Gamma = \frac{\eta_B - \eta}{\eta_B + \eta} \quad (4)$$

where η_B is the intrinsic impedance of the reflective boundary and η is the intrinsic impedance of the media where the antenna is in. For example, the intrinsic impedance of free-space is about 377 Ω. When the reflective boundary is a perfect electrical conductor (PEC), the intrinsic impedance of

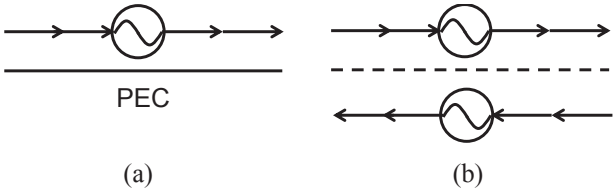

Figure 5. (a) Current flow directions of an antenna on PEC and (b) the respective results after applying image theorem.

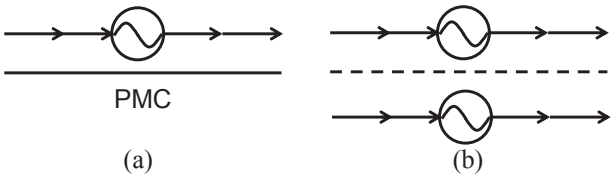

Figure 6. (a) Current flow directions of an antenna on PMC and (b) the respective results after applying image theorem.

the boundary is 0. Thus, the ratio calculated using (4) is -1. On the other hand, when the reflective boundary is a perfect magnetic conductor (PMC), the intrinsic impedance of the boundary is infinity. Thus, the ratio calculated using (4) is 1.

The problems with placing antennas near metallic surfaces are caused because of the composition of out-of-phase waves. Since the resulting reflected waves of metallic surfaces with good conductivity are similar to using PEC as reflective boundary, the ratio calculated by (4) is close to -1. If the antenna is located very close to the reflective boundary, as illustrated in Figure 2, the amplitude of the reflected wave is the same as the radiated wave 1 and the phase has 180° shift compared to the radiated wave 1. The resulting radiation of the antenna is composed of both the radiated wave 1 and the reflected wave. Since the two waves are out-of-phase, the radiation efficiency and the performance of the antenna would degrade severely. This situation can be further explained using the image theorem. As shown in Figure 5, the radiation of an antenna placed on the PEC is the same as replacing the PEC using an image signal with the same amplitude and opposite direction of current flow, at a distance which is same as the distance from the PEC to the original signal. The effective radiation can be viewed as antenna array with two elements. If the distance between the original antenna and the PEC is small, the original signal and the image signal would cancel out. Thus, no power would be transmitted.

To solve the problem, HIS is required to obtain similar results as PMC. By (4), the ratio of E-field is close to 1 if the intrinsic impedance of the reflective boundary is very large. Since the ratio is close to 1, the reflected wave is in-phase. Therefore, instead of canceling out with each other, the reflected wave can enhance the performance of the antenna. As shown in Figure 6, by image theorem, the radiation of an antenna placed on the PMC is the same as replacing the PMC using an image signal with the same amplitude and the same direction of current flow at a distance which is the same as the distance from the PMC to the original signal.

HIS do not have ideal PMC characteristics. The resonance frequency of HIS is affected by the materials near it. Hence, they cannot be placed on any arbitrary set of materials. AMC structure is used to solve this problem. AMC structures are composed of three layers: one layer serves as FSS, one layer

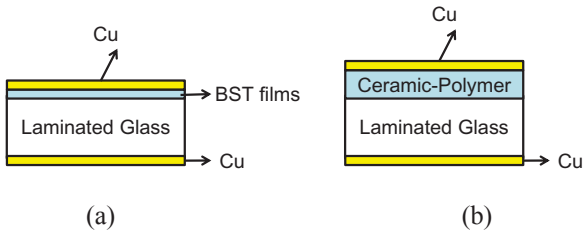

Figure 3. (a) Cross-section of a stackup of AMC with BST thinfilm and (b) cross-section of the stackup of AMC with ceramic-polymer composite.

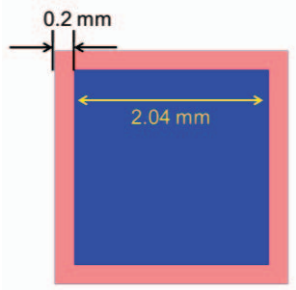

Figure 4. Unit-cell of the square patch AMC.

TABLE I. MATERIAL PROPERTIES OF AMC WITH BST THINFILM

Layer	Thickness (µm)	Dialectic Constant	Loss Tangent
Cu	10		
Laminated Glass	400	5.26	0.0079
BST Film	Case I: 0 Case II: 0.3 Case III: 0.6 Case IV: 3	350	0.05

TABLE II. SUMMARY OF AMC WITH CERAMIC-POLYMER COMPOSITES

Layer	Case V (µm)	Case VI (µm)	Dialectic Constant	Loss Tangent
Cu	10	10		
Laminated Glass	300	0	5.26	0.0079
Ceramic-Polymer	100	400	20	0.005

serves as the spacer, and the third one acts as a metal reflector. Therefore, similar function as the HIS can be obtained using AMC structures. Moreover, the spacer and the metal reflector are used to isolate the structure from other materials, enabling the structure to be placed on the top of any material.

AMCs are effectively comprised of distributed LC networks with inductive impedance at low frequencies to support TM waves, capacitive impedance at high frequencies to support TE waves, and a resonant behavior in the intermediate range, where the structure radiates effectively with no propagation of surface waves. In this frequency range, the structure can also reflect external electromagnetic waves without phase reversal that is usually seen in typical conductors.

B. Modeling and Simulations of AMCs

Full-wave simulations with ANSYS HFSS are used to simulate the performance of nanostructured AMCs. The Master-Slave periodic boundary condition and Floquet ports are used while simulating the structure. The AMC structures

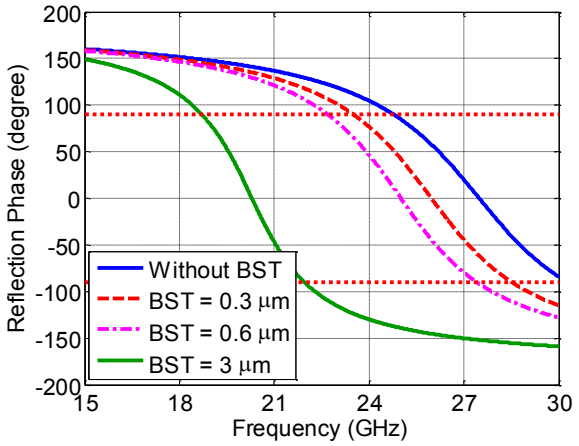

Figure 8. Phase of the reflection coefficient with same unit-cell size but different thicknesses of BST films.

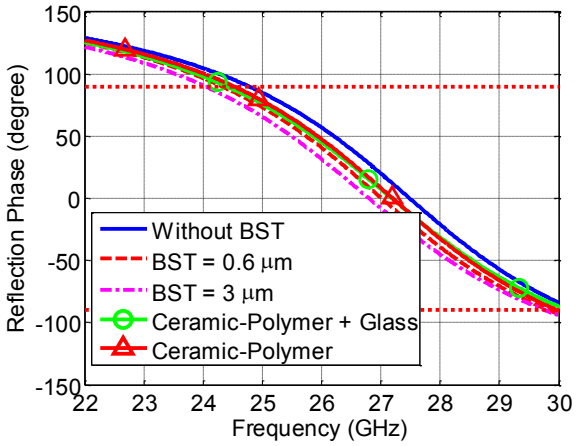

Figure 7. Five different cases with different unit-cell sizes but similar operational frequency.

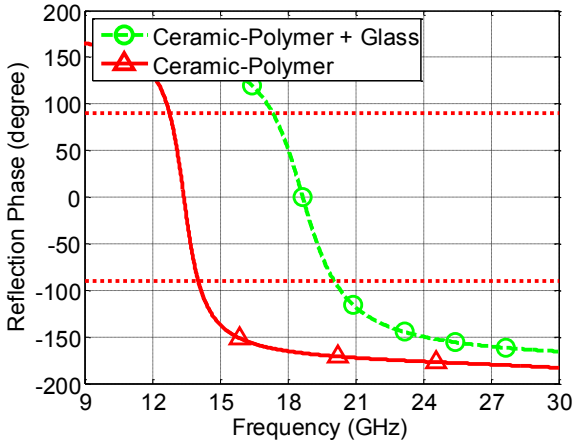

Figure 9. Phase of the reflection coefficient with same unit-cell size but different thicknesses of ceramic-polymer composite film and laminated glass.

TABLE III. AMC UNIT-CELL DIMENSIONS UNDER DIFFERENT CONDITIONS

	Unit-cell size (mm)	Operational Band (GHz)	FBW (%)	Size Reduction Rate
Without BST	2.42	24.5 ~ 30.4	21.5	
0.6 μm BST	2.24	24.3 ~ 29.8	20.3	14.3 %
3 μm BST	1.7	24 ~ 29.8	21.6	50.6 %
Ceramic-Polymer Composite + Glass	1.5	24.4 ~ 30.2	21.3	61.5 %
Ceramic-Polymer Composite	1.16	24.5 ~ 30	20.2	77 %

are characterized by their reflection coefficient. The phase of the reflection is more important than the amplitude of it. The ideal lossless reflection coefficient is 1 and the phase is 0°. The operational band is estimated from -90° to +90° where the incident and reflected waves do not cancel each other.

Two methods to miniaturize the AMC are introduced here. The first one is to insert sub-micron BST thinfilm. A cross-section of the stackup is shown in Figure 3(a). As shown in the figure, the structure is composed of one layer of the top copper plane for the FSS pattern, one layer of BST thinfilm for reducing the size, a layer of laminated glass substrate, and bottom copper plane that serves as the reflector. The thickness and material properties of these materials are summarized in Table I. As demonstrated in Table I, four different thicknesses of BST thinfilms are inserted into the laminated glass to demonstrate the effect of their thickness on the size reduction. The second method is to utilize ceramic-polymer composite films with thickness of ~100 microns. The stackup is shown in Figure 3(b). Two different cases are discussed. Case V uses 100 μm ceramic-polymer composite film and 300 μm of laminated glass. Case VI uses only ceramic-polymer composite film (with no glass substrate) with a thickness of 400 μm, so that the total thicknesses of Case V and Case VI are the same. The material properties and the thicknesses are summarized in Table II. The unit cell of the AMC structure is shown in Figure 4.

The phases of the reflection coefficients for different thicknesses of BST thinfilms are shown in Figure 7. As depicted in Figure 7, with the introduction of BST films, the operation bandwidth shifts to lower frequencies when using the same dimensions of the unit-cell. Moreover, the shift in the frequency band becomes more significant when a thicker BST layer is used. Since the operational band shifts to lower frequencies, a smaller physical area can be used if the same operational band is required. Thus, this suggests an effective size reduction by introducing BST thinfilms. Furthermore, the phases of the reflection coefficients when using ceramic-polymer composites are shown in Figure 8. As depicted in Figure 8, similarly as shown in Figure 7, the operational bands shift to lower frequencies compared with the case which uses only glass without any BST thinfilm. Thus, the size of the AMC can be reduced by utilizing ceramic-polymer composites.

In order to investigate the ratio of the size reduction, five different cases are designed at similar operational band (5G band) and the results are shown in Figure 9. The resulting unit-cell size, operational band, fractional bandwidth (FBW),

and size reduction rates are summarized in Table III. The size reduction rates are calculated using the case without BST thinfilm as reference. As shown in Figure 9, all designs operate at similar frequency bands. Moreover, the operational bandwidths of all three designs are broadband enough to cover the whole 5G bandwidth which is 24.5 GHz to 29.5 GHz. The unit-cell used here is a square. For example, as shown in Table III, the unit-cell size for the case without BST is 2.42 mm, which means an area of 2.42 mm × 2.42 mm. As shown in Table III, with a layer of 3 μm BST thinfilm, 50.6% of the size reduction can be achieved. Besides, the size reduction rate is increased when the thickness of the BST films are increased. Thus, a much more dramatic size reduction is anticipated if thicker BST thinfilm is used. Nevertheless, the operational bandwidth will start to reduce when the thickness of the BST films is too large. Thus, a 3 μm BST thinfilm is a good choice because it reduces the size significantly, while maintaining similar operational bandwidth. On the other hand, size reduction can also be achieved by using ceramic-polymer composites. As shown in Table III, about 60 to 70 % of size reduction can be achieved by using ceramic-polymer composites.

IV. Conclusion

High-impedance surfaces with AMC or FSS are becoming increasingly important for the improvement of antenna performance and noise isolation in emerging ultra-miniaturized 3D antenna-integrated packages. Nanoscale ferroelectrics and ferromagnetics provide unique opportunities to realize such structures. Preliminary modeling analysis with nanoscale BST and ceramic-polymer composites that has frequency-stability bands up to 30 GHz is demonstrated in this paper. About 60 to 70 % size reduction can be accomplished by applying ceramic-polymer composites with hundreds of micron thickness. Moreover, the size of AMCs can be reduced even for ultra-thin BST films. The size reduction rate with only 3 μm BST is 50.6 %. Besides, by extending this approach to thicker dielectric films as well as to nanomagnetics, further miniaturization is feasible. This approach can be extended to lower frequency bands using nanomagnetic composite films for pervasive applications. Such nanostructured materials and structures represent 10-20X enhancement in frequencies compared to the state-of-the-art and can be potentially applied to numerous applications in 5G, IoT, and smart skin domains.

References

[1] S. Borkar and H. Pande, "Application of 5G next generation network to Internet of Things," in *2016 International Conference on Internet of Things and Applications (IOTA)*, 2016, pp. 443-447.

[2] G. Haubner, W. Hartner, S. Pahlke, and M. Niessner, "77GHz automotive RADAR in eWLB package: From consumer to automotive packaging," *Microelectronics Reliability*, vol. 64, pp. 699-704, 2016.

[3] J. Min, Z. Wu, M. R. Pulugurtha, V. Smet, V. Sundaram, A. Ravindran, et al., "Modeling Design Fabrication and Demonstration of RF Front-End Module with Ultra-Thin Glass Substrate for LTE Applications," in *Electronic Components and Technology Conference (ECTC), 2016 IEEE 66th*, 2016, pp. 1297-1302.

[4] L. Ragan, A. Hassibi, T. S. Rappaport, and C. L. Christianson, "Novel on-chip antenna structures and frequency selective surface (FSS) approaches for millimeter wave devices," in *Vehicular Technology Conference,* 2007. VTC-2007 Fall. 2007 IEEE 66th, 2007, pp. 2051-2055.

[5] M. De Cos, F. Las Heras, and M. Franco, "Design of planar artificial magnetic conductor ground plane using frequency-selective surfaces for frequencies below 1 GHz," *IEEE Antennas and Wireless Propagation Letters*, vol. 8, pp. 951-954, 2009.

[6] S. Gandhi, M. R. Pulugurtha, H. Sharma, P. Chakraborti, and R. R. Tummala, "High-$ k $ Thin-Film Capacitors With Conducting Oxide Electrodes on Glass Substrates for Power-Supply Applications," *IEEE Transactions on Components, Packaging and Manufacturing Technology*, vol. 6, pp. 1561-1566, 2016.

[7] T. Moon, B. Lee, T.-G. Kim, J. Oh, Y. W. Noh, S. Nam, et al., "Microwave dielectric relaxation of the polycrystalline (Ba, Sr) Ti O 3 thin films," *Applied Physics Letters*, vol. 86, p. 182904, 2005.

[8] J. Baniecki, R. Laibowitz, T. Shaw, P. Duncombe, D. Neumayer, D. Kotecki, et al., "Dielectric relaxation of Ba 0.7 Sr 0.3 TiO 3 thin films from 1 mHz to 20 GHz," *Applied physics letters*, vol. 72, pp. 498-500, 1998.

[9] L. M. Malkinski, M. Yu, A. Y. Vovk, D. J. Scherer II, L. Spinu, W. Zhou, et al., "Microwave absorption of patterned arrays of nanosized magnetic stripes with different aspect ratios," *Journal of Applied Physics*, vol. 101, p. 09J110, 2007.